ACS OMEGA

http://pubs.acs.org/journal/acsodf

Article

Experimental Investigation of Supercritical CO_2–Rock–Water Interactions in a Tight Formation with the Pore Scale during CO_2–EOR and Sequestration

Yulong Zhang, Leiting Shi,* Zhongbin Ye, Liang Chen, Na Yuan, Ying Chen, and Hao Yang

Cite This: *ACS Omega* 2022, 7, 27291–27299

Read Online

ACCESS | Metrics & More | Article Recommendations

ABSTRACT: In recent years, gas injection, especially CO_2 injection, has been acknowledged as a promising approach for enhanced oil recovery (EOR) and CO_2 capture and storage (CCS), especially for tight reservoirs. However, when CO_2 is injected into the oil reservoirs, it can disturb the equilibrium of the system and lead to chemical reactions between CO_2, formation water, and reservoir rocks. The reactions will alter some geochemical and physicochemical characteristics of the target reservoirs. However, the reactions still lack quantitative characterization at the pore scale, especially under reservoir conditions. Herein, we conducted an experimental study of the interactions between CO_2, brine, and rocks in the Mahu oilfield at 20 MPa and 70 °C. The low-field nuclear magnetic resonance (LF-NMR) measurements showed that the incremental amplitude for tight cores of CO_2–rock–water tests was larger than that for CO_2–rock tests, and the amplitude alteration presented significant differences corresponding to different types of minerals and pores. Furthermore, the interplanar spacing of the core samples was increased with the increase of reaction time in the CO_2–rock experiments but still lower than that in CO_2–rock–water tests. This research demonstrated evident changes in the geochemistry in tight reservoirs caused by CO_2, brine, and rock reactions. The results of this study may provide a significant reference for the exploration of similar reservoirs in the field of CO_2–EOR and CO_2 sequestration.

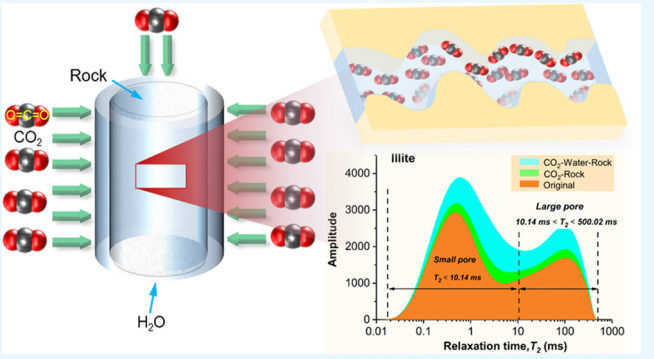

INTRODUCTION

Unconventional reservoirs including tight oil and shale oil have been drawing increasing attention owing to the increasing energy demand. According to the estimation, approximately 30 billion barrels of unconventional oil are distributed worldwide in 24 oil reservoirs.[1−3] The recoveries of these reservoirs (Bakken oilfield, Eagle Ford oilfield, and Vaca Muerta oilfield) are believed to be less than 10% even after fracture, owing to their low porosity and ultralow permeability.[4,5] Therefore, enhanced oil recovery (EOR) approaches should be applied to disclose the locking.[6,7] The commonly used water flooding is not suitable for tight reservoirs (Bakken oilfield and Eagle Ford oilfield) owing to the extra high injection pressure.[8] CO_2 flooding has been proven to be useful and had the potential to enhance the recovery of tight reservoirs (Bakken oilfield, Eagle Ford oilfield, and Changqing oilfield) among all of the effective EOR methods.[9−11] In addition, reducing CO_2 emissions has become an urgent worldwide problem. Thus, CO_2–EOR associated with CO_2 sequestration illustrated an excellent development potential in the future.[12]

It was concluded that the equilibrium of the natural condition would be broken owing to the injection of CO_2 into the subterranean layer. Subsequently, the alteration of geochemical and physicochemical features of the target reservoirs would change due to the chemical reaction among reservoir rocks and formation brine and consequently affect the behavior of CO_2–EOR.[13−15] Therefore, it is of vital importance to have a comprehensive understanding of the reactions triggered by the injection of CO_2. Lots of efforts have been devoted to studying the interactions of CO_2–water–rock in recent years.

Zhang et al. investigated the interactions of reservoir rocks (Lucaogou formation of Jimsar sag, Junggar Basin), formation brine, and supercritical CO_2 under reservoir conditions. They found that the dissolving of supercritical CO_2 in the formation water would generate an acidic condition, which would cause the dissolving of minerals and their subsequent precipitation.

Received: April 11, 2022
Accepted: July 19, 2022
Published: July 29, 2022

Table 1. Petrophysical Properties of the Core Samples

scenarios	tests	length (cm)	diameter (cm)	permeability, K_{air} (mD)	porosity, Φ (%)
CO_2−core	1 (calcite)	6.57	2.54	0.09	8.11
	2 (kaolinite)	6.41	2.54	0.12	9.26
	3 (illite)	6.26	2.53	0.07	8.04
	4 (feldspar)	6.39	2.54	0.08	8.21
CO_2−water−core	5 (calcite)	6.52	2.51	0.06	8.07
	6 (kaolinite)	6.29	2.54	0.10	8.96
	7 (illite)	6.28	2.54	0.07	8.13
	8 (feldspar)	6.40	2.54	0.09	8.19

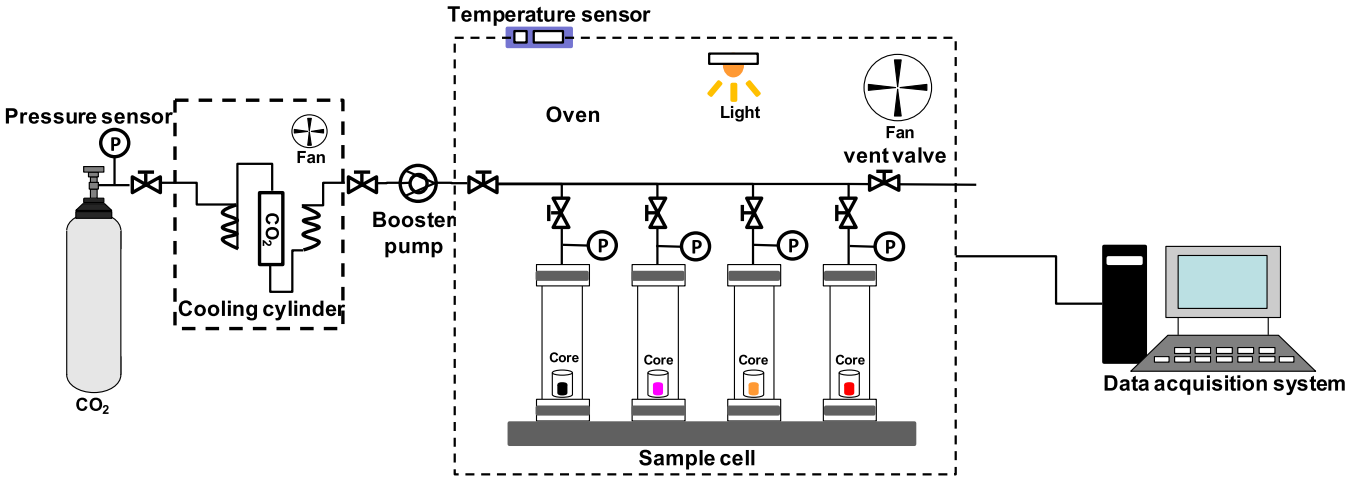

Figure 1. Schematic of the experimental setup for CO_2 and cores experiments.

Furthermore, the rock surface after exposure to CO_2 was changed to be hydrophilic owing to mineral dissolving, kaolinite formation, and surface corrosion.[13] Abedini et al. claimed that the chemical interactions might lead to dissolution and precipitation of certain minerals and alter the geophysical properties, including porosity and permeability of reservoir rocks.[16] Yu et al. claimed that mineral wettability, composition, and oil saturation were the main controls on the exposed surface area of grains, and mineral wettability, in particular, led to selective dissolution.[17] Fuchs et al. evaluated the effects of geochemical reactions on the geomechanical integrity of representative siliciclastic reservoir samples. The fracture toughness results demonstrated that carbon storage reservoirs might undergo geomechanical weakening with CO_2 injection, which could lead to redistribution of stresses that are able to induce fracture slippage and trigger microseismic events.[18] Zou et al. found that mineral dissolutions caused numerous large etched pores, which eventually resulted in a significant increase in porosity and permeability in their experiment.[19] Zhang et al. utilized computed tomography (CT) scanning-discrete element method (DEM) combined approach to explore the alterations of limestone rock mechanical properties during CO_2 injection.[20] Wei et al. investigated the interaction dynamics between CO_2, water, and rock minerals under realistic reservoir conditions. The results indicated that CO_2-triggered reactions increased the permeability of the tight core, leading to the consumption of injected CO_2.[8] Tang et al. explored the mechanism that alters the characteristics of the reservoir for the CO_2−brine−rock reaction during CO_2 injection and storage in gas reservoirs. The results showed that the interaction resulted in the alteration of petrophysical properties that core permeability reduced as the porosity increased. Therefore, the dry CO_2 ought to be injected into the water area to decrease the side effect of CO_2−brine−rock interactions and guarantee the practical implementation of CO_2 capture and storage (CCS) projects in gas reservoirs with the aquifer.[21] However, few researchers have investigated the effects of different minerals on CO_2−water−rock interactions at the pore scale in a realistic reservoir environment. Actually, it is vital to investigate the mineral types suitable for CO_2 storage.

Owing to the extremely low permeability of the tight reservoir, little efforts have been devoted to exploring the reactions between CO_2 and rock minerals at the pore scale. Moreover, most of the existing studies failed to quantify the impacts of the interactions between CO_2, water, and rock minerals. Therefore, this work focuses on quantifying the alterations caused by the interactions between CO_2, tight core, and water of the Mahu tight conglomerate reservoir in the Junggar Basin, northwest China, under reservoir conditions (20 MPa, 70 °C) at the pore scale. X-ray diffraction (XRD), scanning electron microscopy (SEM), and low-field nuclear magnetic resonance (LF-NMR) spectroscopy were applied to characterize the reaction process in this study. The LF-NMR measurement results indicated that the increase of amplitude for tight cores of CO_2−rock−water tests was mostly higher than that of CO_2−rock tests. The increase of amplitude for big pores was higher than that for small pores in the case of CO_2−rock trials, while the opposite results were observed in CO_2−rock−water tests. Furthermore, the amplitude alteration presented great differences corresponding to different types of minerals and pores. Notable alteration of the mineral surface could be observed in SEM analysis owing to the interaction between CO_2, water, and rock. The XRD measurements of the

https://doi.org/10.1021/acsomega.2c02246
ACS Omega 2022, 7, 27291−27299

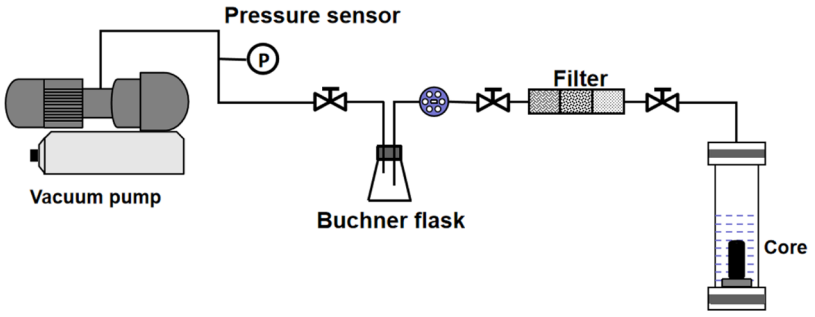

Figure 2. Schematic illustration of the experimental setup for the vacuum saturation device.

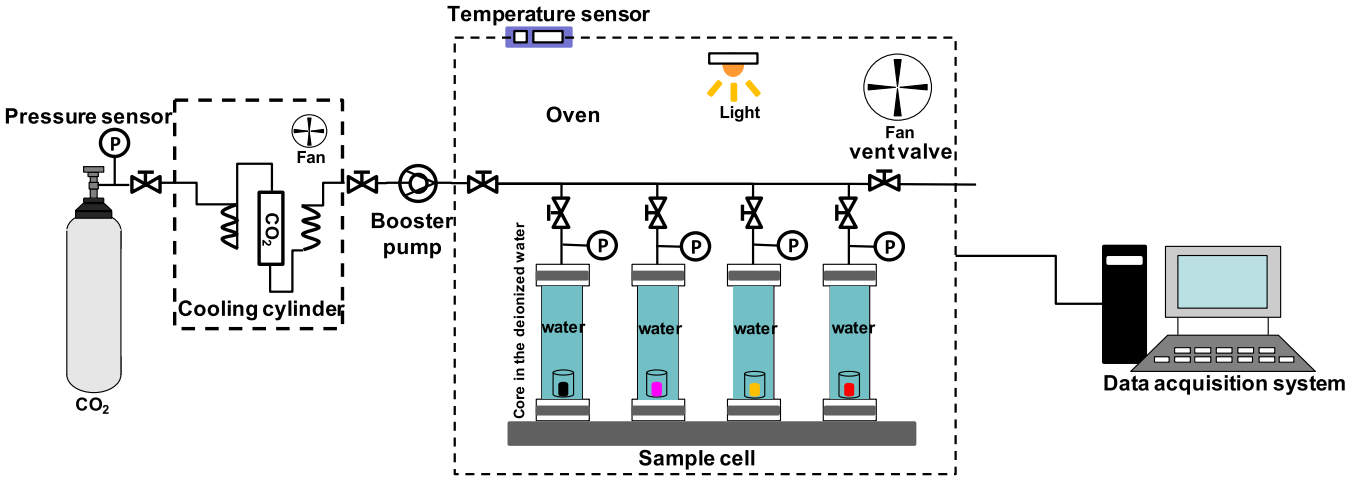

Figure 3. Schematic illustration of the experimental setup for different tight cores soaked in supercritical carbon dioxide (SC-CO_2) under deionized water.

cores also indicated that the saturated CO_2 could further expand the pore size. The research of this paper offered a further explanation of the CO_2–EOR and CCS in tight reservoirs.

EXPERIMENTAL METHODS

Materials. Synthetic core samples with pure minerals (calcite, feldspar, illite, kaolinite) were prepared before the tests. Then, they were dried in an oven at 100 °C for more than 90 h to diminish the influence of water before gas permeability and porosity measurements (LkiQR-168 Jiangsu Haian Petroleum Scientific Research Instrument Co., Ltd., China). The petrophysical characteristics of the used core are shown in Table 1. The deionized water was used in tests 5–8, and the CO_2 was sourced from CO_2 cylinders with a purity of 99.99%.

Reaction between CO_2 and Cores. The experimental process is described as follows: (1) vacuuming of the system and (2) injection of CO_2 into the high temperature–high pressure (HT–HP) (Hastelloy, Haian Petroleum Technology Co.) cell at 20 MPa and 70 °C until equilibrium. The schematic diagram of the process is shown in Figure 1.

Reaction between CO_2, Cores, and Deionized Water. The core samples were first soaked in deionized water for 72 h, as shown in Figure 2. Then, they were placed in the HT–HP cell, as illustrated in Figure 3. The experimental procedures are briefly described as follows: (1) the HT–HP cell was filled with deionized water; (2) the temperature was increased to 70 °C and air was vacuumed from the whole system, and then CO_2 was pumped into the reference cell and pressurized to 5.0 MPa until the pressure was stable for 1 h; (3) the valve was opened and CO_2 was injected into the HT–HP cell to a pressure of 20 MPa for 10 days; and (4) the mass loss of the core before and after the reaction was calculated. The percentage of mass loss was calculated as follows

$$W_t = (W_b - W_a)/W_b \quad (1)$$

where W_t stands for the percentage of mass loss of the rock, W_b is the weight of the rock after reaction (g), and W_b represents the weight of the rock before the reaction (g).

Scanning Electron Microscopy (SEM) Analysis. A core piece was cut from the end face of the tight core before and after being soaked in the supercritical carbon dioxide (SC-CO_2). The morphology of core tablets was observed by scanning electron microscopy (SEM) with a FEI Quanta 450.

Low-Field Nuclear Magnetic Resonance (LF-NMR) Test. The core plugs were subjected to vacuum at 10^{-1} MPa for one week using a vacuum pressurization saturation device (KDZB-II, Kedi, China) and then pressurized to 30 MPa to saturate the core with brine (room temperature). Then, the cores were subjected to LF-NMR spectrometry (AniMR-150, Shanghai Niumag Electronic Technology Co., Ltd., China) to conduct the measurements of the nuclear magnetic resonance (NMR) T_2 spectrum. The permanent magnet of the NMR spectrometer is 0.23 ± 0.03 T with a resonance frequency of 12 MHz. The echo and scanning numbers were 18 000 and 64, respectively. All of the measurements were performed at room temperature and atmospheric pressure.

https://doi.org/10.1021/acsomega.2c02246
ACS Omega 2022, 7, 27291–27299

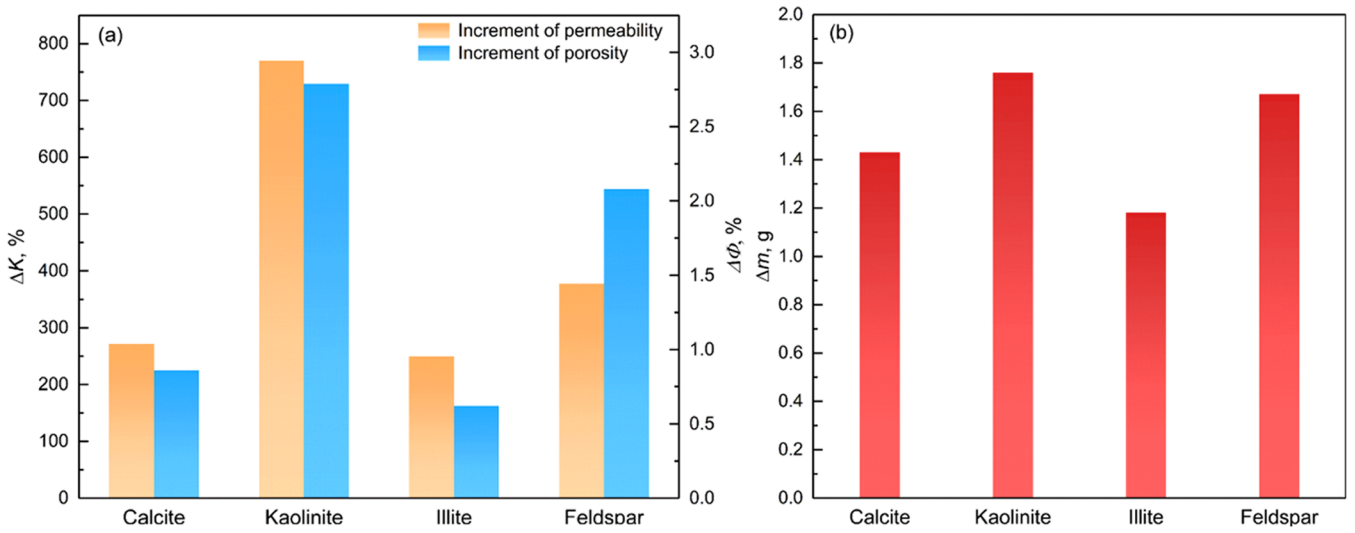

Figure 4. Porosity/permeability increment (a) and mass loss (b) of the core sample after the interaction between CO_2, water, and rock.

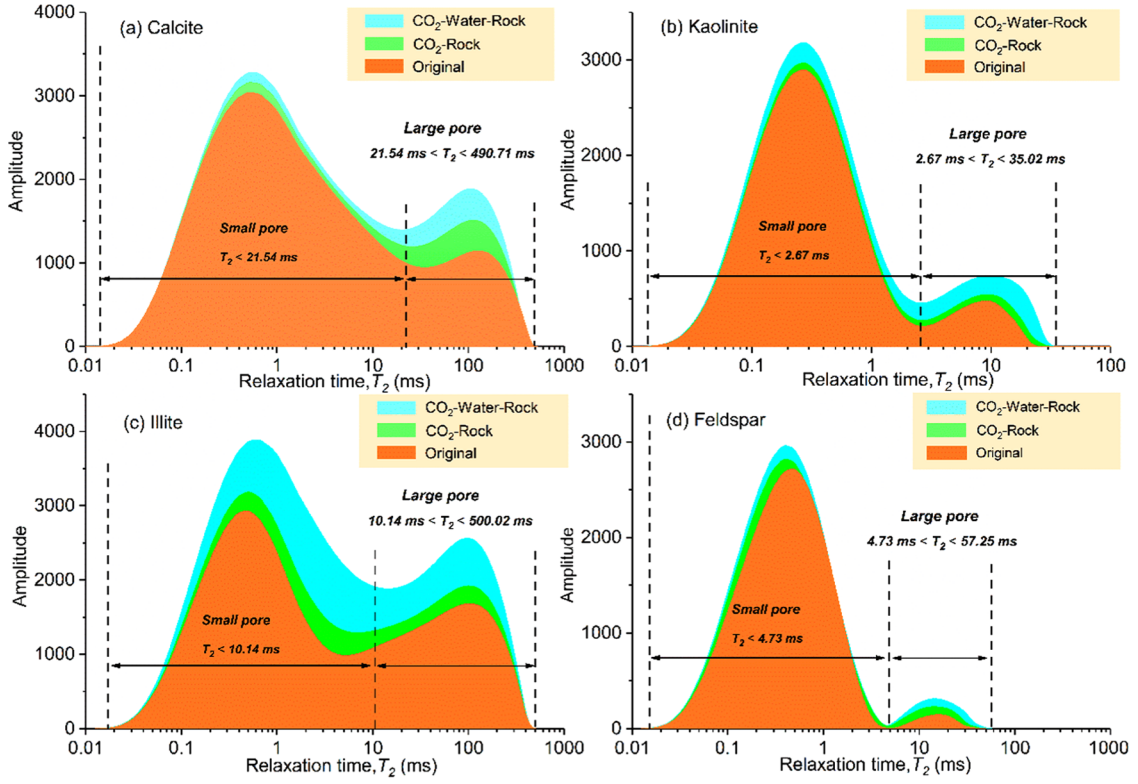

Figure 5. NMR T_2 spectra of different cores ((a) calcite, (b) kaolinite, (c) illite, (d) feldspar) during CO_2−rock and CO_2−rock−water measurements.

RESULTS AND DISCUSSION

LF-NMR Analysis. To comprehensively describe the CO_2−rock−water interactions, low-field nuclear magnetic resonance (LF-NMR) was applied to illustrate the reaction process. The NMR transverse relaxation time (T_2) spectra of the original, CO_2−rock, CO_2−rock−water for cores with different mineral types are presented in Figure 5. Based on the bimodal T_2 curve, the pores of the tight cores can be divided into two regimes (small pores and large pores).[22−24] The increase of amplitude for tight cores of CO_2−rock−water tests was mostly higher than that for CO_2−rock tests owing to the dissolution reaction.[25] Figure 7 simply presents the mechanisms of altering the pore size before and after the test. In the case of CO_2−rock reaction tests, CO_2 was trapped in porous media primarily through the adsorption process, and it could slightly enlarge the pore size of tight cores. However, this effect was not as strong as expected even though the CO_2 was under a supercritical state. By contrast, the significant increase of pore size caused by the dissolution reaction is much more obvious than that by CO_2−rock tests. Furthermore, it was found that the increase of amplitude for big pores was much higher than that for small pores in CO_2−rock−water tests, as shown in Figure 6. This might be due to the fact that there was a large amount of micropores in tight cores, which were helpful

https://doi.org/10.1021/acsomega.2c02246
ACS Omega 2022, 7, 27291−27299

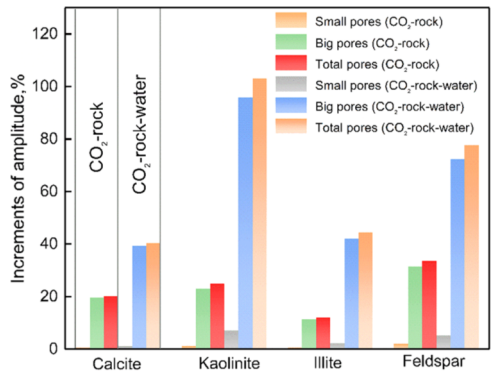

Figure 6. Increments of amplitude with different cores during CO_2–rock and CO_2–rock–water measurements in different pore intervals.

to the dissolution interactions between CO_2, rock, and water. The dispersed micropores were well connected after being exposed to saturated CO_2. It should be noted that the alteration of amplitude presented significant differences corresponding to different types of minerals and pores. The highest increase of amplitude of total pores and big pores occurred in feldspar during the CO_2–rock test.[26] But in the case of CO_2–water–rock measurements, the highest increase of amplitude of total pores and big pores occurred in kaolinite. The mass loss and permeability/porosity alterations of tight cores after CO_2–water–rock tests also present the same results, as shown in Figure 4 (Figures 5, 6, and 7).

Mineral Surfaces. Figure 8 shows the mineral surface morphology of the rock disks before and after the CO_2–water–rock reaction by SEM. It can be seen that the rock consisted of fine cemented minerals, as shown in Figure 8a. After being exposed to saturated CO_2, the dissolved pores and pits were clearly observed, which could notably increase the connectivity of the tight reservoir rocks, as shown in Figure 8b.[27] Furthermore, the SEM images presented conclusive evidence of feldspar dissolution (Figure 8b) and kaolinization (Figure 8d).

XRD Analysis. It can be seen from Figure 9 that the intensities of the peaks become notably weak with the increase of reaction time, which corresponds to the expansion of the mineral during the injection of CO_2. New characteristic peaks were not observed during the experiments, indicating that only physical interaction was triggered between CO_2 and tight core. On the contrary, the new characteristic peaks occurred in the case of CO_2–water–rock experiments (as shown in Figure 10), which suggested that there existed a chemical reaction during the injection of saturated CO_2. Furthermore, the interplanar spacing D, which can comprehensively reflect the alteration of the pore size of the cores before and after the injection of CO_2/saturated CO_2 was calculated by the following equation

$$D = \frac{K\lambda}{B\cos\theta} \tag{2}$$

where K is the Scherrer constant, λ denotes the wavelength of X-ray, B represents the half-width of the peak for the core samples, and θ is the diffraction angle.

It can be seen from Tables 2–5 that the interplanar spacing of the core samples was increased with the increase of reaction time in the CO_2–rock experiments but still lower than that in CO_2–rock–water tests. This may be attributed to the expansion of pore size being limited since only physical interactions occurred during the injection of CO_2. In contrast, the chemical reaction caused by the injection of saturated CO_2 could further expand the pore size.

CONCLUSIONS

To clarify the interaction process between CO_2, water, and rock at the pore level during the CO_2–EOR operations, we systematically presented an experimental investigation of characterizing the reaction mechanism in tight cores under reservoir conditions using LF-NMR, XRD, and SEM methods. Based on the experimental data, the following conclusions can be generally drawn:

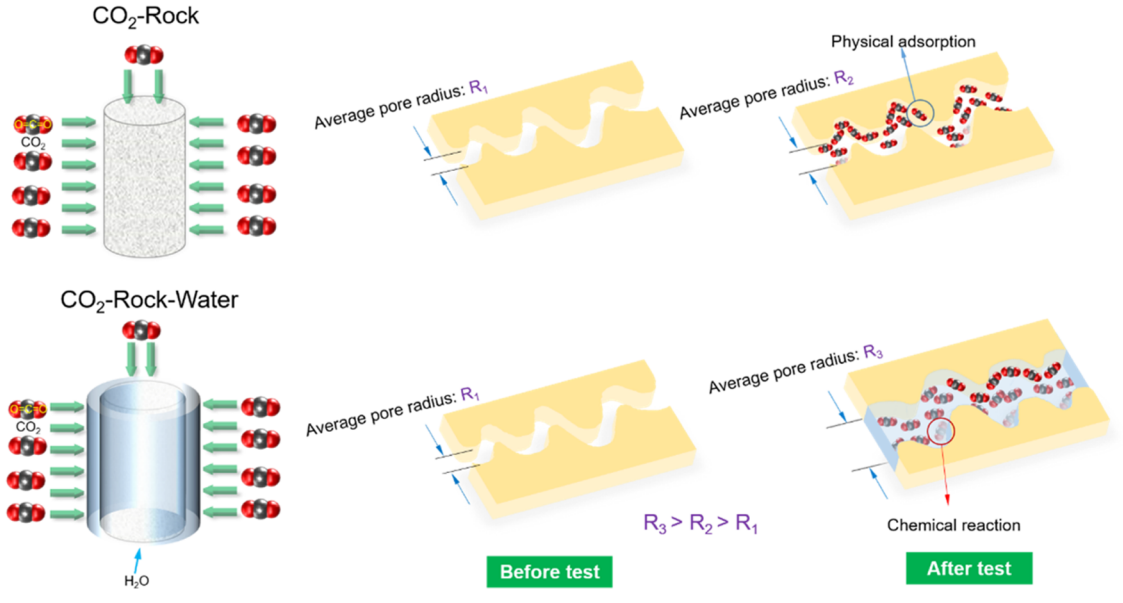

Figure 7. Schematic of the alteration mechanisms of pore size during CO_2–rock and CO_2–rock–water measurements.

https://doi.org/10.1021/acsomega.2c02246
ACS Omega 2022, 7, 27291–27299

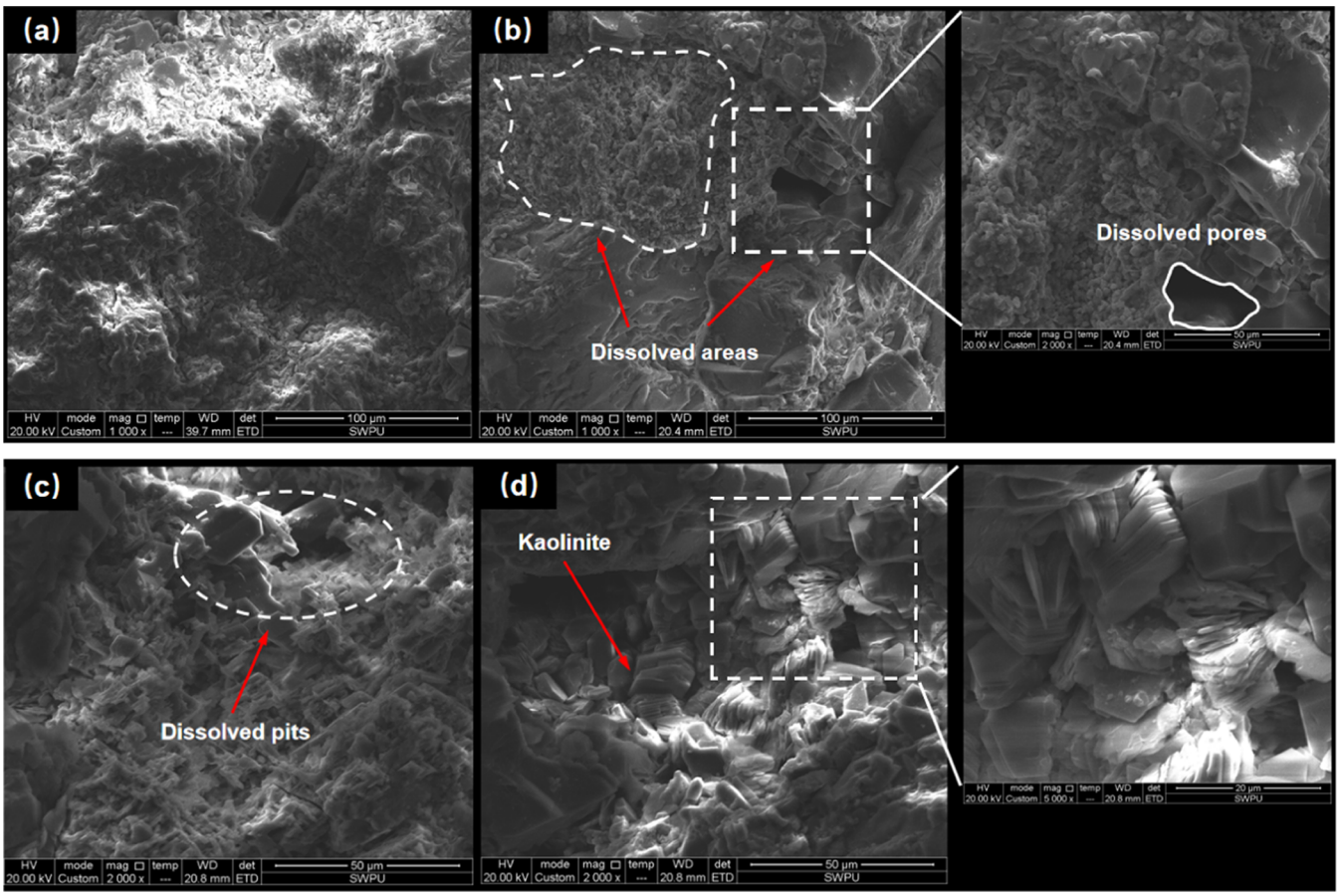

Figure 8. Mineral surface morphology of the rock disks before (a) and after the CO_2−water rock reaction (b−d).

(a) The low-field NMR tests indicated that the increase of amplitude for CO_2−rock−water tests was larger than that for CO_2−rock tests due to the dissolution reaction.

(b) The amplitude alteration presented great differences corresponding to different types of minerals and pores.

(c) The interplanar spacing of the core samples was increased with the reaction time in the CO_2−rock experiments but was still lower than that in CO_2−rock−water tests.

(d) Although limited works have been conducted in this paper, it provides some insights into the study of CO_2−EOR and CCS in tight reservoirs. For example, core samples with a single mineral in this study were not representative to reflect the actual reservoir condition. Therefore, the natural cores will be used to characterize the CO_2−EOR process at the pore scale in our future works.

AUTHOR INFORMATION

Corresponding Author

Leiting Shi − *State Key Laboratory of Oil and Gas Reservoir Geology and Exploitation, Southwest Petroleum University, Chengdu, Sichuan 610500, China;* orcid.org/0000-0001-9530-5760; Email: zhangxiangswpu@139.com

Authors

Yulong Zhang − *State Key Laboratory of Oil and Gas Reservoir Geology and Exploitation, Southwest Petroleum University, Chengdu, Sichuan 610500, China*

Zhongbin Ye − *Chengdu Technological University, Chengdu 611730, China*

Liang Chen − *Geological exploration and Development Research Institute of CNPC Chuanqing Drilling Engineering Co., Ltd, Chengdu 610051, China*

Na Yuan − *Exploitation and Development Research Institute, PetroChina Daqing Oilfield Company, Daqing 163000, China*

Ying Chen − *Chongqing Natural Gas Purification Plant General, Petrochina Southwest Oil & Gas field Company, Chongqing 400000, China*

Hao Yang − *No. 2 Gas Production Plant, SINOPEC Southwest Oil and Gas Company, Langzhong, Sichuan 637400, China*

Complete contact information is available at: https://pubs.acs.org/10.1021/acsomega.2c02246

Notes

The authors declare no competing financial interest.

ACKNOWLEDGMENTS

The authors gratefully acknowledge the financial support of Research and Innovation Fund for Postgraduates of SWPU (2020CXZD28). The authors also thank the anonymous reviewers for their valuable comments.

NOMENCLATURE

EOR = enhanced oil recovery
CCS = CO_2 capture and storage

https://doi.org/10.1021/acsomega.2c02246
ACS Omega 2022, 7, 27291−27299

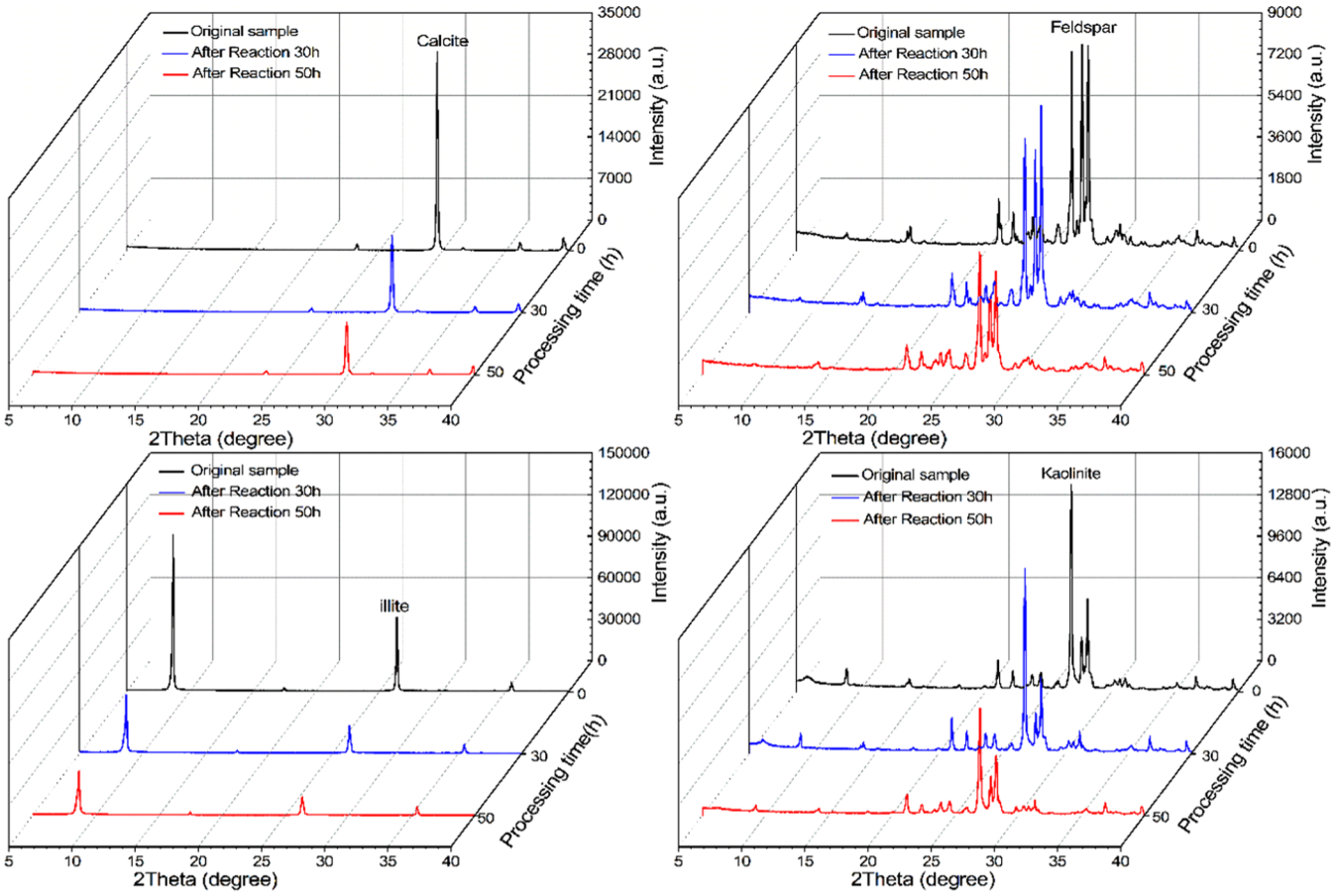

Figure 9. XRD spectra of different cores during CO_2−rock experiments.

NMR = nuclear magnetic resonance
LF-NMR = low-field nuclear magnetic resonance
XRD = X-ray diffraction
CT = computed tomography
SEM = scanning electron microscopy
DEM = discrete element method
SC-CO_2 = supercritical carbon dioxide
B = half-width of peak
θ = diffraction angle
T_2 = NMR transverse relaxation time
D = interplanar spacing
K_{air} = permeability to air
K = Scherrer constant
Φ = porosity, %

REFERENCES

(1) Abedini, A.; Torabi, F. Oil recovery performance of immiscible and miscible CO_2 Huff-and-puff processes. *Energy Fuels* **2014**, *28*, 774−784.

(2) Pu, W.; Wei, B.; Jin, F.; Li, Y.; Jia, H.; Liu, P.; Tang, Z. Experimental investigation of CO_2 huff-n-puff process for enhancing oil recovery in tight reservoirs. *Chem. Eng. Res. Des.* **2016**, *111*, 269−276.

(3) Ren, B.; Zhang, L.; Huang, H.; Ren, S.; Chen, G.; Zhang, H. Performance evaluation and mechanisms study of near-miscible CO_2 flooding in a tight oil reservoir of Jilin Oilfield China. *J. Nat. Gas Sci. Eng.* **2015**, *27*, 1796−1805.

(4) Liu, J.; Sheng, J. J. Investigation of Countercurrent Imbibition in Oil-Wet Tight Cores Using NMR Technology. *SPE J.* **2020**, *25*, 2601−2614.

(5) Wei, B.; Zhang, X.; Wu, R.; Zou, P.; Gao, K.; Xu, X.; Pu, W.; Wood, C. Pore-scale monitoring of CO_2 and N_2 flooding processes in a tight formation under reservoir conditions using nuclear magnetic resonance (NMR): A case study. *Fuel* **2017**, *246*, 34−41.

(6) Bealessio, B. A.; Alonso, N. A. B.; Mendes, N. J.; Sande, A. V.; Hascakir, B. A review of enhanced oil recovery (EOR) methods applied in Kazakhstan. *Petroleum* **2021**, *7*, 1−9.

(7) Wei, B.; Lu, L.; Pu, W.; Wu, R.; Zhang, X.; Li, Y.; Jin, F. Production dynamics of CO_2 cyclic injection and CO_2 sequestration in tight porous media of Lucaogou formation in Jimsar sag. *J. Pet. Sci. Eng.* **2017**, *157*, 1084−1094.

(8) Wei, B.; Zhang, X.; Liu, J.; Xu, X.; Pu, W.; Bai, M. Adsorptive behaviors of supercritical CO_2 in tight porous media and triggered chemical reactions with rock minerals during CO_2-EOR and -sequestration. *Chem. Eng. J.* **2020**, *381*, No. 122577.

(9) Zhang, C.; Li, Z.; Sun, Q.; Wang, P.; Wang, S.; Liu, W. CO_2 foam properties and the stabilizing mechanism of sodium bis(2-ethylhexyl)sulfosuccinate and hydrophobic nanoparticle mixtures. *Soft Matter* **2016**, *12*, 946−956.

(10) Zhou, X.; Yuan, Q.; Rui, Z.; Wang, H.; Feng, J.; Zhang, L.; Zeng, F. Feasibility study of CO_2 huff 'n' puff process to enhance heavy oil recovery via long core experiments. *Appl. Energy* **2019**, *236*, 526−539.

(11) Lee, H.; Oncel, N.; Liu, B.; Kukay, A.; Altincicek, F.; Varma, R. S.; Shokouhimehr, M.; Ostadhassan, M. Structural Evolution of Organic Matter in Deep Shales by Spectroscopy (1H and 13C Nuclear Magnetic Resonance, X-ray Photoelectron Spectroscopy, and Fourier Transform Infrared) Analysis. *Energy Fuels* **2020**, *34*, 2807−2815.

(12) Lee, H.; Shakib, F. A.; Shokouhimehr, M.; Bubach, B.; Kong, L.; Ostadhassan, M. Optimal Separation of CO_2/CH_4/Brine with Amorphous Kerogen: A Thermodynamics and Kinetics Study. *J. Phys. Chem. C* **2019**, *123*, 20877−20883.

https://doi.org/10.1021/acsomega.2c02246
ACS Omega 2022, 7, 27291−27299

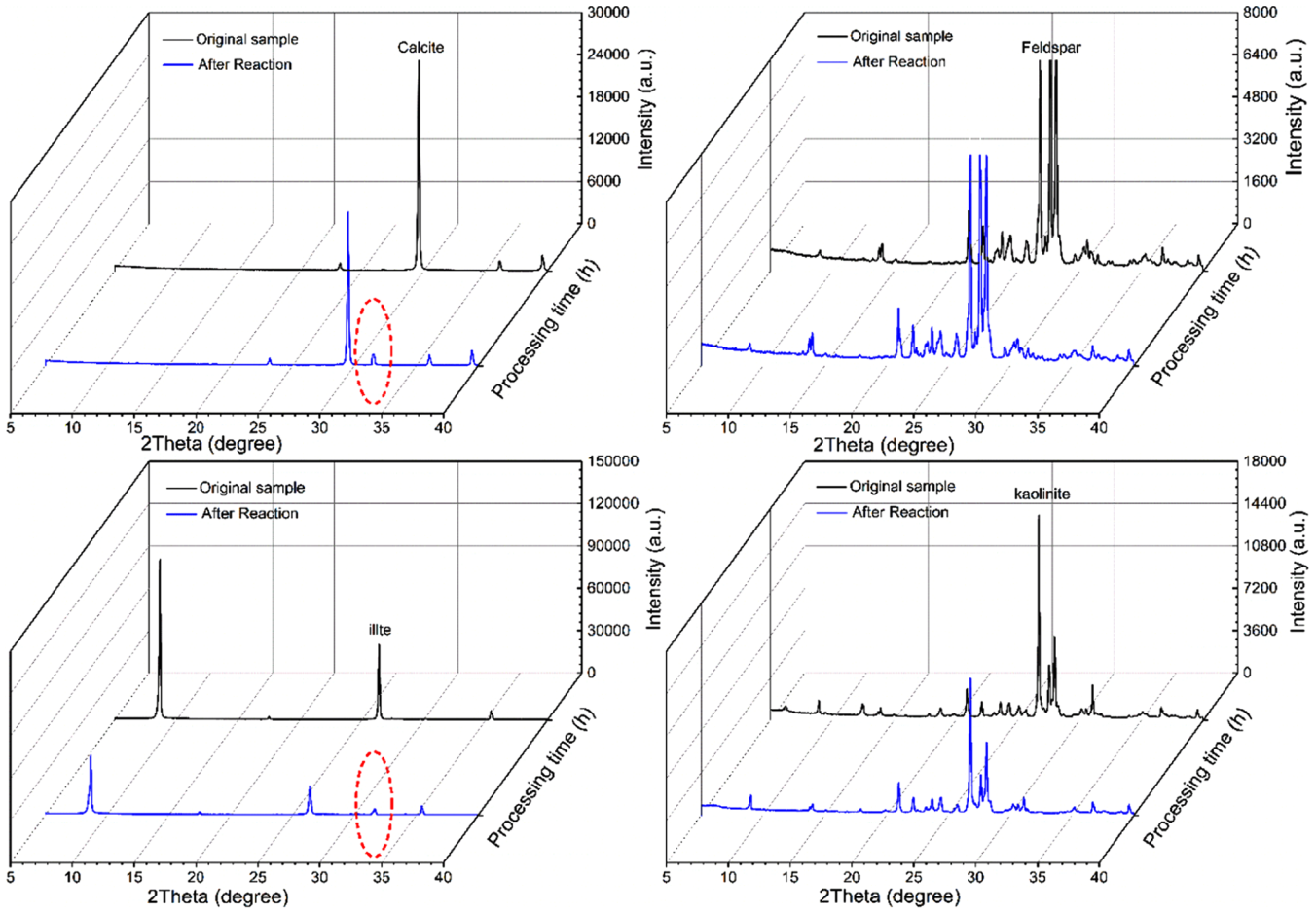

Figure 10. XRD spectra of different cores during CO_2–rock–water experiments.

Table 2. Parameters of XRD during Calcite–CO_2 and Calcite–CO_2–Water Tests

calcite–CO_2	D (interplanar spacing, nm)	B (half-width of peak)	2θ
origin	0.2987	0.204	29.5904
30 h	0.3001	0.179	29.7604
50 h	0.3016	0.147	29.8964
calcite–CO_2–water	0.3026	0.154	29.4954

Table 3. Parameters of XRD during Feldspar–CO_2 and Feldspar–CO_2–Water Tests

feldspar–CO_2	D (interplanar spacing, nm)	B (half-width of peak)	2θ
origin	0.3138	0.492	28.114
30 h	0.3152	0.262	28.128
50 h	0.3168	0.205	29.264
feldspar–CO_2–water	0.3234	0.155	28.051

Table 4. Parameters of XRD during Kaolinite–CO_2 and Kaolinite–CO_2–Water Tests

kaolinite–CO_2	D (interplanar spacing, nm)	B (half-width of peak)	2θ
origin	0.3599	0.204	26.7854
30 h	0.3619	0.164	26.8346
50 h	0.3628	0.162	27.0064
kaolinite–CO_2–Water	0.3657	0.17	26.7584

Table 5. Parameters of XRD during Illite–CO_2 and Illite–CO_2–Water Tests

illite–CO_2	D (interplanar spacing, nm)	B (half-width of peak)	2θ
origin	1.0107	0.148	8.6966
30 h	1.1343	0.133	8.7096
50 h	1.1661	0.132	8.7266
illite–CO_2–water	1.1674	0.129	8.6836

(13) Zhang, X.; Wei, B.; Shang, J.; Gao, K.; Pu, W.; Xu, X.; Wood, C.; Sun, L. Alterations of geochemical properties of a tight sandstone reservoir caused by supercritical CO_2-brine-rock interactions in CO_2-EOR and geosequestration. *J. CO_2 Util.* **2018**, *28*, 408–418.
(14) Foroozesh, J.; Jamiolahmady, M. The physics of CO_2 transfer during carbonated water injection into oil reservoirs: From non-equilibrium core-scale physics to field-scale implication. *J. Pet. Sci. Eng.* **2018**, *166*, 798–805.
(15) Zhang, X.; Ranjith, P. G. Experimental investigation of effects of CO_2 injection on enhanced methane recovery in coal seam reservoirs. *J. CO_2 Util.* **2019**, *33*, 394–404.
(16) Abedini, A.; Torabi, F. On the CO_2 storage potential of cyclic CO_2 injection process for enhanced oil recovery. *Fuel* **2014**, *124*, 14–27.
(17) Yu, M.; Liu, L.; Yang, S.; Yu, Z.; Li, S.; Yang, Y.; Shi, X. Experimental identification of CO_2-oil-brine-rock interactions: Implications for CO_2 sequestration after termination of a CO_2-EOR project. *Appl. Geochem.* **2016**, *75*, 137–151.
(18) Fuchs, S. J.; Espinoza, D. N.; Lopano, C. L.; Akono, A. T.; Werth, C. J. Geochemical and geomechanical alteration of siliciclastic reservoir rock by supercritical CO_2-saturated brine formed during

https://doi.org/10.1021/acsomega.2c02246
ACS Omega 2022, 7, 27291–27299

geological carbon sequestration. *Int. J. Greenhouse Gas Control* **2019**, *88*, 251−260.
(19) Zou, Y.; Li, S.; Ma, X.; Zhang, S.; Li, N.; Chen, M. Effects of CO_2−brine−rock interaction on porosity/permeability and mechanical properties during supercritical-CO_2 fracturing in shale reservoirs. *J. Nat. Gas Sci. Eng.* **2018**, *49*, 157−168.
(20) Zhang, Y.; Zhang, Z.; Arif, M.; Lebedev, M.; Busch, A.; Sarmadivaleh, M.; Iglauer, S. Carbonate rock mechanical response to CO_2 flooding evaluated by a combined X-ray computed tomography − DEM method. *J. Nat. Gas Sci. Eng.* **2020**, *84*, No. 103675.
(21) Tang, Y.; Hu, S.; He, Y.; Wang, Y.; Wan, X.; Cui, S.; Long, K. Experiment on CO_2-brine-rock interaction during CO_2 injection and storage in gas reservoirs with aquifer. *Chem. Eng. J.* **2021**, *413*, No. 127567.
(22) Dang, S. T.; Sondergeld, C. H.; Rai, C. S. Interpretation of nuclear-magnetic-resonance response to hydrocarbons: Application to miscible enhanced-oil-recovery experiments in shales. *SPE Reservoir Eval. Eng.* **2019**, *22*, 302−309.
(23) Huang, X.; Li, A.; Li, X.; Liu, Y. Influence of Typical Core Minerals on Tight Oil Recovery during CO_2 Flooding Using the Nuclear Magnetic Resonance Technique. *Energy Fuels* **2019**, *33*, 7147−7154.
(24) Wang, H.; Lun, Z.; Lv, C.; Lang, D.; Luo, M.; Zhao, Q.; Zhao, C. Nuclear-Magnetic-Resonance Study on Oil Mobilization in Shale Exposed to CO_2. *SPE J.* **2020**, *25*, 432−439.
(25) Su, X.; Yue, X. A. Mechanism study of the relation between the performance of CO_2 immiscible flooding and rock permeability. *J. Pet. Sci. Eng.* **2020**, *195*, No. 107891.
(26) Gao, Z.; Feng, J.; Cui, J.; Wang, X.; Zhou, C.; Shi, Y. Physical simulation and quantitative calculation of increased feldspar dissolution pores in deep reservoirs. *Pet. Explor. Dev.* **2017**, *44*, 387−398.
(27) Cui, G.; Yang, L.; Fang, J.; Qiu, Z.; Wang, Y.; Ren, S. Geochemical reactions and their influence on petrophysical properties of ultra-low permeability oil reservoirs during water and CO_2 flooding. *J. Pet. Sci. Eng.* **2021**, *203*, No. 108672.

https://doi.org/10.1021/acsomega.2c02246
ACS Omega 2022, 7, 27291−27299